Effect of resonant and non-resonant magnetic braking on error field tolerance in high beta plasmas

H. Reimerdes[1,a], A.M. Garofalo[2], E.J. Strait[2], R.J. Buttery[3], M.S. Chu[2], Y. In[4], G.L. Jackson[2], R.J. La Haye[2], M.J. Lanctot[1], Y.Q. Liu[3], M. Okabayashi[5], J.-K. Park[5], M.J. Schaffer[2] and W.M. Solomon[5]

[1] Department of Applied Physics and Applied Mathematics, Columbia University, New York, NY 10027, USA
[2] General Atomics, PO Box 85608, San Diego, CA 92186-5608, USA
[3] EURATOM/UKAEA Fusion Association, Culham Science Centre, Abingdon, Oxfordshire OX14 3DB, UK
[4] FAR-TECH, Inc., San Diego, CA 92121, USA
[5] Princeton Plasma Physics Laboratory, Princeton, NJ 08543-0451, USA

E-mail: reimerdes@fusion.gat.com

Abstract

Tokamak plasmas become less tolerant to externally applied non-axisymmetric magnetic 'error' fields as beta increases, due to a resonant interaction of the non-axisymmetric field with a stable $n = 1$ kink mode. Similar to observations in low beta plasmas, the limit to tolerable $n = 1$ magnetic field errors in neutral beam injection heated H-mode plasmas is seen as a bifurcation in the torque balance, which is followed by error field-driven locked modes and severe confinement degradation or a disruption. The error field tolerance is, therefore, largely determined by the braking torque resulting from the non-axisymmetric magnetic field. DIII-D experiments distinguish between a resonant-like torque, which decreases with increasing rotation, and a non-resonant-like torque, which increases with increasing rotation. While only resonant braking leads to a rotation collapse, modelling shows that non-resonant components can lower the tolerance to resonant components. The strong reduction of the error field tolerance with increasing beta, which has already been observed in early high beta experiments in DIII-D (La Haye *et al* 1992 *Nucl. Fusion* **32** 2119), is linked to an increasing resonant field amplification resulting from a stable kink mode (Boozer 2001 *Phys. Rev. Lett.* **86** 5059). The amplification of externally applied $n = 1$ fields is measured with magnetic pick-up coils at normalized beta values as low as 1 and seen to increase with beta. The rate at which the amplification increases with beta becomes larger above the no-wall ideal MHD stability limit, where kinetic effects stabilize the resistive wall mode. The extent of the beta dependence and its importance for low torque scenarios was not previously appreciated, and was not included in the empirical scaling of the error field tolerance for ITER, which focused on the lowest density phase of a discharge prior to H-mode access (Buttery *et al* 1999 *Nucl. Fusion* **39** 1827, 1999 ITER Physics Basis *Nucl. Fusion* **39** 2137). However, the measurable increase in the plasma response with beta can be exploited for 'dynamic' correction (i.e. with slow magnetic feedback) of the amplified error field.

PACS numbers: 52.30.−q, 52.30.Cv, 52.35.Py, 52.55.Fa, 52.55.Tn

(Some figures in this article are in colour only in the electronic version)

1. Introduction

Tokamak plasmas are very sensitive to non-axisymmetric perturbations of the magnetic equilibrium field. These non-axisymmetric fields usually arise from small but unavoidable misalignments of the axisymmetric poloidal and toroidal magnetic field coils and the presence of non-axisymmetric coil feeds and are referred to as *error* fields. External perturbations as small as $\delta B^{\text{ext}}/B_{\text{T}} \approx 10^{-4}$, where B_{T} is the toroidal magnetic field, can lead to locked modes

[a] Author to whom any correspondence should be addressed.

in Ohmically heated, L-mode plasmas and to rotation and pressure collapses in neutral beam injection (NBI) heated H-mode discharges. While the error field tolerance is usually described by empirical scaling laws [1, 2], which are based on Ohmic locked mode experiments and depend mainly on the electron density n_e (e.g. [3–5]), early high β experiments in DIII-D, with $\beta \equiv 2\mu_0\langle p\rangle/B_T^2$ being the normalized volume averaged plasma pressure, already showed a strong reduction of the error field tolerance at high values of β [6]. The $n = 1$ error field threshold in discharges that exceed the ideal MHD no-wall stability limit was initially interpreted as a stability threshold with magnetic braking leading to a loss of rotational stabilization and, consequently, an unstable resistive wall mode (RWM). However, it has recently been pointed out that, similar to the low β locked mode experiments, the $n = 1$ error field tolerance of high β plasmas is caused by a bifurcation in the torque balance [7]. This work investigates the role of magnetic braking in determining the error field tolerance of high β plasmas. Section 2 shows that the $n = 1$ error field tolerance is determined by 'resonant' magnetic braking, explains the β dependence of the error field tolerance with the role of the plasma response, discusses the difference between *pitch-resonant* and *kink-resonant* external fields, demonstrates the beneficial effect of toroidal torque input and draws the link to low β experiments. Section 3 looks in detail at the magnetic braking caused by the plasma response to external fields revealing the importance of non-resonant effects. Section 4 summarizes the findings and discusses the consequences for ITER.

2. Error field tolerance of high beta plasmas

The error field tolerance is systematically studied in controlled magnetic braking experiments, where non-axisymmetric coils deliberately apply a well-known error field. The magnetic braking is applied in weakly shaped, lower-single null H-mode discharges ($B_T = 2.0$ T, $I_p = 1.1$ MA, $q_{95} \approx 5.0$, $q_{\min} \approx 1.5$), which have advanced tokamak relevant q-profiles but low ideal MHD no-wall β limits. The plasmas are heated with up to 12 MW of tangential NBI with beamlines pointing in both toroidal directions, which decouples the NBI heating power P_{NBI} from the NBI torque T_{NBI} and allows for independent control of the plasma β and rotation. The experiments take advantage of the flexible non-axisymmetric control coil sets and extensive magnetic perturbation diagnostics on DIII-D. The plasma shape and the poloidal location of the control coils and of the toroidal arrays of magnetic sensors are shown in figure 1. While a set of six control coils in the mid-plane outside the vacuum vessel (C-coils) is used to empirically correct the $n = 1$ component of the intrinsic error field, two sets of six control coils each (I-coils) located above and below the outboard mid-plane inside the vacuum vessel apply the well-known external $n = 1$ perturbation. The difference between the toroidal phases of the $n = 1$ field applied with the upper and the lower I-coil arrays $\Delta\phi_I$ can be varied to modify the pitch or poloidal spectrum of the externally applied field. The I-coil is usually configured with a phase difference $\Delta\phi_I = 240°$, where 1 kA of $n = 1$ current typically generates a pitch-resonant external normal field at the location of the $q = 2$ surface of $\delta B_{21}^{ext} \approx 1.0$ G.
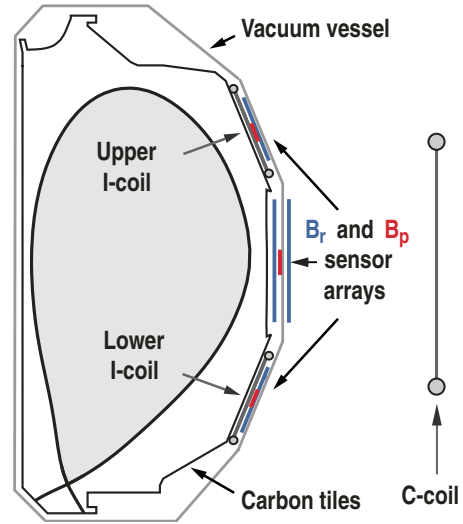
Figure 1. Poloidal cross-section of a weakly shaped lower-single null plasma used in the error field tolerance study and the DIII-D vessel with the location of I-coils, C-coils and various arrays of magnetic sensors.

External fields are generated by currents outside the plasma and are also referred to as *vacuum* fields. Various toroidal arrays of pick-up coils and saddle loops measure the perturbed poloidal and radial fields δB_p and δB_r. Subtracting the known vacuum coupling from the magnetic measurements yields the corresponding plasma response δB_p^{plas} and δB_r^{plas}, which is the magnetic field caused by the perturbed currents in the plasma. The magnetic measurements shown in this paper have been obtained exclusively with the poloidal field probes at the outboard mid-plane, figure 1.

2.1. Torque balance and error field penetration

In order to study the relation between magnetic braking and error field tolerance, the I-coil currents are programmed to generate a slowly rotating (10 Hz) $n = 1$ field whose amplitude increases on a time scale that is slow compared with a typical angular momentum confinement time τ_L of 50 ms, figures 2(*a*) and (*b*). The slow toroidal rotation facilitates the extraction of the plasma response to the externally applied non-axisymmetric field from magnetic and various other measurements, while inducing only negligible eddy currents in the wall. As the $n = 1$ field is ramped up, the toroidal plasma angular rotation Ω, which is measured with charge exchange recombination (CER) spectroscopy using C VI emission, decreases, figure 2(*c*), and the $n = 1$ plasma response δB_p^{plas}, measured with a toroidal array of poloidal magnetic field probes at the outboard mid-plane increases steadily, figure 2(*d*). During this first phase of the magnetic braking process, which lasts until $t = 2910$ ms, the electron temperature T_e, figure 2(*e*), measured with an electron cyclotron emission (ECE) diagnostic, does not show any signatures of magnetic islands that could be driven by the external field. At $t = 2910$ ms the rotation starts to decrease more rapidly, which is referred to as a rotation collapse. The collapse is followed by an error field-driven locked mode, which is now seen as a cylical broadening of the T_e contours in
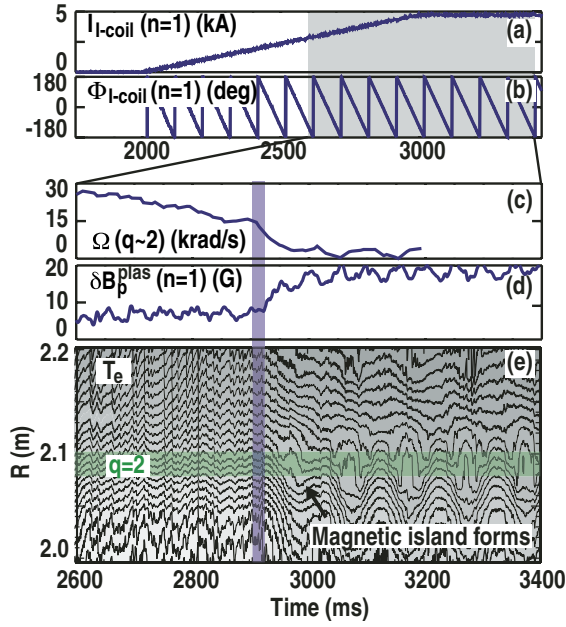
Figure 2. Programmed evolution of (*a*) the amplitude $I_{\text{I-coil}}$ and (*b*) toroidal phase $\phi_{\text{I-coil}}$ of $n = 1$ currents in the I-coil leads to magnetic braking of (*c*) the toroidal plasma rotation Ω and an increase in (*d*) the $n = 1$ plasma response $\delta B_{\text{p}}^{\text{plas}}$. (*e*) Contours of the electron temperature T_{e} show evidence of the formation of a magnetic island after the plasma rotation has collapsed.

the vicinity of the $q = 2$ surface as the externally applied field rotates the magnetic island past the ECE diagnostic [8]. The characteristics of the error field limit in these high β H-modes are similar to the observations in low-density, locked mode experiments in Ohmically heated L-mode plasmas (e.g. [4]). It is understood that a sufficiently large plasma flow through the perturbed field induces helical currents at the rational surfaces $q = m/n$, which shield the pitch-resonant harmonics of the externally applied field and suppress the formation of islands [9]. The finite resistivity leads to dissipation and consequently a toroidal torque, which is referred to as a resonant magnetic braking torque. The evolution of the plasma rotation can be described by

$$I\frac{\mathrm{d}\Omega}{\mathrm{d}t} = T_{\text{in}} - \frac{I\Omega}{\tau_{\text{L},0}} - T_{\text{MB}}, \qquad (1)$$

where I is the moment of inertia, T_{in} the sum of all accelerating torques and $\tau_{\text{L},0}$ the momentum confinement time in the absence of non-axisymmetric fields. When the magnetic braking torque T_{MB} increases sufficiently fast with decreasing Ω, the torque balance can be lost and the rotation collapses [9]. If T_{MB} is proportional to Ω^{-1}, which is typical for a resonant magnetic braking torque, the torque balance equation (1) predicts this bifurcation to occur at a critical rotation $\Omega_{\text{crit}} = T_{\text{in}}\tau_{\text{L},0}/(2I)$. If T_{in} is kept constant and $\tau_{\text{L},0}$ remains constant, this corresponds to half of the unperturbed rotation, $\Omega_{\text{crit}} = \Omega_0/2$. When the plasma rotation is too low to induce the helical shielding currents, the error field penetrates and an island opens, consistent with the observations, as shown in figure 2. In DIII-D the characteristic relation between Ω_{crit} and Ω_0 has been observed in several plasma scenarios and over a wide range of rotation values

[7, 10]. The external non-axisymmetric magnetic field and the corresponding plasma response immediately prior to the rotation collapse are identified as the tolerable (or critical) external field $\delta B_{s,\text{crit}}^{\text{ext}}$ and the tolerable plasma response $\delta B_{s,\text{crit}}^{\text{plas}}$, where the index s denotes the component and/or location of the perturbed field.

While resonant braking, which leads to a loss of torque balance and subsequently error field penetration, can describe the limit to externally applied $n = 1$ fields over a wide range of parameters, $n = 1$ field ramps at high β and low NBI torque usually lead to the onset of a $m/n = 2/1$ neoclassical tearing mode (NTM) before the rotation collapses. These modes are typically born rotating but quickly lock. The observation of 2/1 NTMs at high β and low rotation is consistent with the reduction of the 2/1 NTM β_{N} threshold with decreasing rotation in the direction of the plasma current observed in sawtoothing H-mode discharges [11]. It is, therefore, plausible that non-axisymmetric fields affect the NTM stability primarily through braking of the plasma rotation. However, it is also thought that non-axisymmetric fields can directly reduce the NTM β_{N} threshold [12]. The NTM stability boundary limits the present study of the $n = 1$ error field tolerance at high β_{N} and low Ω.

2.2. Dependence of error field tolerance on beta and role of plasma response

The dependence of the $n = 1$ error field tolerance on β_{N} is measured in similar discharges with β_{N} ranging from 1.5 to 2.3. Stability calculations using the ideal MHD stability code DCON [13] yield a no-wall stability limit $\beta_{\text{N,nw}}$ of approximately 2.0 corresponding to $2.5\ell_{\text{i}}$, where ℓ_{i} is the internal inductance. In this shot-to-shot scan the NBI heating power P_{NBI} is varied independently of the NBI torque T_{NBI}. The values of P_{NBI} and T_{NBI} are determined from a Monte-Carlo calculation of the collisional slowing of fast beam ions within the TRANSP code [14]. A comparison of two discharges with $T_{\text{NBI}} = 1.8\,\text{N}\,\text{m}$ shows that a 33% increase in β_{N} from 1.5 to 2.0, figure 3(*a*), halves the tolerable externally applied field $\delta B_{21,\text{crit}}^{\text{ext}}$, figure 3(*b*). At higher β_{N} a smaller externally applied field leads to a similar rotation decay and the rotation collapse occurs at approximately the same rotation, figure 3(*c*). However, at higher β_{N} the $n = 1$ plasma response $\delta B_{\text{p}}^{\text{plas}}$ to the externally applied field is also larger resulting in the same plasma response at the time of the rotation collapse of $\delta B_{\text{p,crit}}^{\text{plas}} \approx 6.9\,\text{G}$, figure 3(*d*). The continuation of the β_{N} scan at a higher value of $T_{\text{NBI}} \approx 4.0\,\text{N}\,\text{m}$ shows that the rate of the decrease in the error field tolerance with β_{N} becomes even larger when β_{N} approximately exceeds the no-wall limit, figure 4(*a*). Again the plasma response to the externally applied field $\delta B_{\text{p,crit}}^{\text{plas}} \approx 9.7\,\text{G}$ remains independent of β_{N}, figure 4(*b*). The resulting increase in the ratio of plasma response and non-axisymmetric coil current $\delta B_{\text{p,crit}}^{\text{plas}}/I_{\text{I-coil}}$ with β_{N} at high values of β_{N}, shown in figure 4(*c*) for discharges with various values of NBI torque, has been observed in several devices [15–17] and is attributed to resonant amplification of a weakly stable $n = 1$ kink mode [18]. The amplification is particularly large when β_{N} exceeds the ideal MHD no-wall stability limit and kinetic effects are thought to result in a stable, but only weakly damped RWM [19]. Consistent with
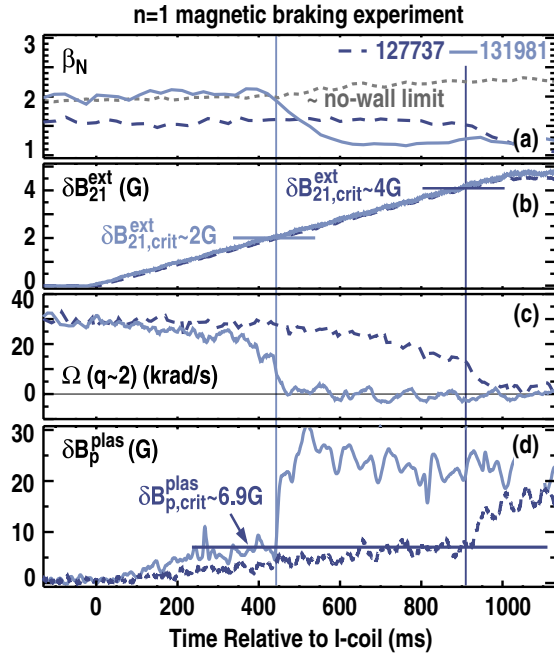
Figure 3. Comparison of magnetic braking in two discharges with different values of β_N, but constant NBI torque $T_{NBI} \approx 1.8$ N m, including the evolution of (*a*) β_N and the approximate no-wall limit (dotted), (*b*) the resonant component of the external $n = 1$ field at the $q = 2$ surface δB_{21}^{ext}, (*c*) the toroidal rotation Ω at the $q = 2$ surface and (*d*) the measured plasma response δB_p^{plas}. Vertical lines indicate the start of the rotation collapse. (Colour online.)

expectations for an error field tolerance that is determined by the loss of torque balance, the tolerable plasma perturbation $\delta B_{p,crit}^{plas}$ increases with T_{NBI}, as shown in figure 4(*b*). The observed β_N dependence of the tolerance to externally applied $n = 1$ fields can, therefore, be explained by the β_N dependence of the amplification of external fields and a magnetic braking torque that is determined by the plasma response rather than the externally applied (vacuum) perturbation and that leads to a loss of torque balance.

2.3. Dependence of the error field tolerance on the poloidal spectrum

The dependence of the $n = 1$ error field tolerance on the poloidal spectrum of the externally applied field is investigated by probing similar plasmas ($\beta_N \approx 2.2$, $T_{NBI} = 4.5$ N m) with I-coil fields that differ from the standard phase difference of $\Delta\phi_I = 240°$. The corresponding poloidal harmonics of the normal component of the external field calculated using a straight-field-line coordinate based on a typical target equilibrium are shown in figure 5. For $\Delta\phi_I = 120°$ the external field has a spectral peak with a dominant right-handed helicity ($m > 0$), whereas the equilibrium field is left-handed ($m < 0$), figure 5(*a*). For $\Delta\phi_I = 180°$ the external field is well aligned with the equilibrium field at the outboard mid-plane maximizing the resonant component, figure 5(*b*). The good alignment of the spectral peak with the equilibrium field along the radius is a manifestation of the medium aspect ratio tokamak characteristic that the pitch of field lines at the outboard mid-plane remains approximately constant across
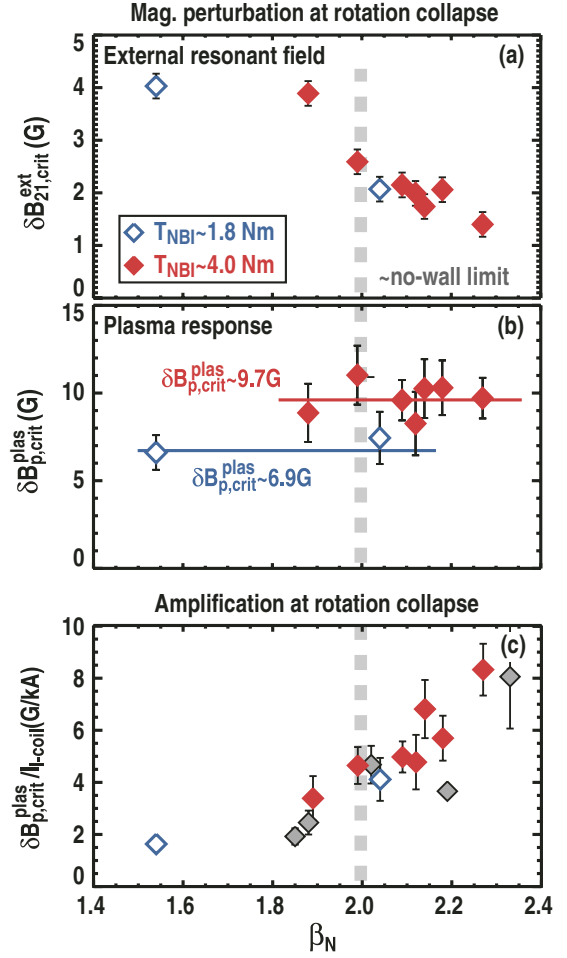
Figure 4. Dependence of (*a*) the tolerable external resonant field $\delta B_{21,crit}^{plas}$ and (*b*) the corresponding measured $n = 1$ plasma response $\delta B_{p,crit}^{plas}$ on the value of β_N for discharges with constant NBI torque $T_{NBI} \approx 1.8$ N m (open blue) and 4.0 N m (filled red). The β_N dependence of the tolerable external field and of the corresponding plasma response are linked through the β_N dependence of the plasma amplification, here (*c*) evaluated as the ratio of $\delta B_{p,crit}^{plas}$ and the I-coil current I_{I-coil} at the rotation collapse and including discharges with other values of T_{NBI} (filled grey). The dashed vertical line indicates an estimate of the ideal MHD no-wall stability limit. (Colour online.)

large parts of the plasma radius. For $\Delta\phi_I = 240°$ the external field has a lower pitch angle than the equilibrium field yielding a peak of the poloidal mode spectrum for $|m| > q$, figure 5(*c*).

Reducing $\Delta\phi_I$ from 240° to 180° allows approximately for a doubling of the externally applied resonant field at the $q = 2$ surface δB_{21}^{ext} before the rotation collapses, figure 6(*a*). In the case of $\Delta\phi_I = 120°$ the currents in the I-coil can even be ramped up to the power-supply-limited maximum current of 4.5 kA, increasing δB_{21}^{ext} by another 50%, while causing only modest braking and no rotation collapse. Again the braking is not related to the external resonant field, but to the plasma response. The rotation collapse occurs when the plasma response reaches $\delta B_{p,crit}^{plas} \approx 10$ G, independent of the I-coil phase difference, figure 6(*a*). In the case of $\Delta\phi_I = 120°$ the plasma response remains below the critical value and consequently no rotation collapse occurs. The coupling of currents in the I-coil with the $\Delta\phi_I = 240°$
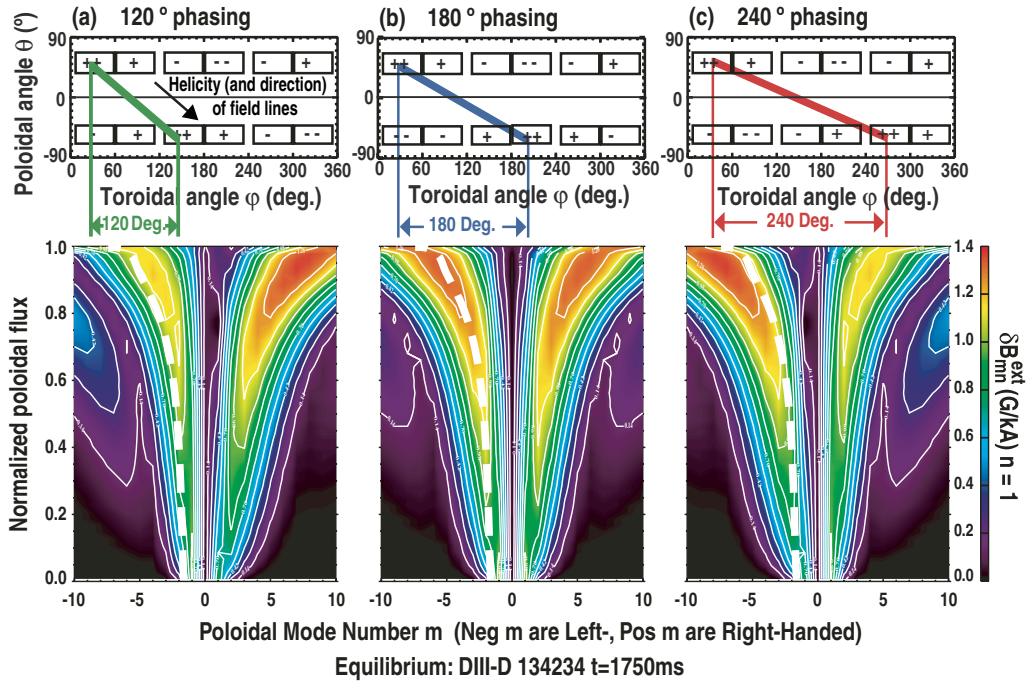
Figure 5. Poloidal harmonics m in straight-field-line coordinates of the normal external field $\delta B_{mn}^{\text{ext}}$ inside the plasma for $n = 1$ I-coil configurations with phase differences between the upper and lower arrays $\Delta\phi_{\text{I}}$ of 120° (*a*), 180° (*b*) and 240° (*c*). The vertical axis is a radial coordinate (normalized poloidal flux) and the dashed curve indicates the local resonant component of the external field. For the discharges used in this study the I-coil configuration with $\Delta\phi_{\text{I}} = 180°$ maximizes the resonant component of the external field.

configuration to the plasma is approximately six times more effective than the coupling to currents with the $\Delta\phi_{\text{I}} = 120°$ configuration, figure 6(*b*). At the same time the component of the externally applied field that is resonant with the pitch of the equilibrium field at the $q = 2$ surface $\delta B_{21}^{\text{ext}}$ shows a weak maximum for the $\Delta\phi_{\text{I}} = 180°$ configuration, with $\delta B_{21}^{\text{ext}}$ for $\Delta\phi_{\text{I}} = 120°$ and $\Delta\phi_{\text{I}} = 240°$ being approximately the same. The correlation between the plasma response and the pitch-resonant components of the external field on other resonant surfaces is equally poor, which shows that the plasma does not dominantly respond to the pitch-resonant component of the external field.

The interaction of non-axisymmetric fields with the plasma can be modelled with the MARS-F code [20]. It is thought that the stabilization of the RWM above the ideal MHD no-wall stability limit is a result of kinetic effects [19], but the present implementation of semi-kinetic stabilization in MARS-F [21] still falls short of a quantitative description of the experimental observations [10]. While a quantitative prediction of the damping rate, and hence amplification, is not expected, the code can describe the coupling of external fields to the stable kink mode. The $n = 1$ plasma response at the location of the δB_{p} measurements is calculated for I-coil fields with various phase differences $\Delta\phi_{\text{I}}$, figure 6(*b*). The equilibrium of discharge 134234 at $t = 1750$ ms is ideal MHD unstable and sound wave damping [22] is added to stabilize the plasma. The strength of the sound wave damping is adjusted by setting the free coefficient in the parallel viscosity $\kappa_{\parallel} = 1$ in order to match the measured plasma response for $\Delta\phi_{\text{I}} = 120°$. Varying only $\Delta\phi_{\text{I}}$ yields the largest coupling for $\Delta\phi_{\text{I}} = 300°$. The MARS-F calculation correctly describes the observed large increase in the coupling when $\Delta\phi_{\text{I}}$ is increased from 120°

to 240°. The large coupling for $\Delta\phi_{\text{I}} = 300°$ is not unexpected, since for this I-coil phase difference the external field at the wall best matches the pattern of kink or RWM as can be seen from MARS-F calculation of the RWM structure shown in figure 7. The kink mode is more sensitive to external fields with higher m components than the equilibrium field, since it is at these high left-handed $|m| > q$ components, where the spectrum of the 240° configuration peaks, figure 5(*c*), while the spectrum of the 120° configuration is particularly depressed, figure 5(*a*). The modelling confirms that the plasma response is correlated with the component of the externally applied field that is 'resonant' with the kink mode and not the component that is resonant with pitch of the equilibrium field inside the plasma. A plasma response amplifying an externally applied $n = 1$ field has also been detected below the no-wall limit at values of β_{N} as low as 1.0. The plasma response at these intermediate values of β_{N} has similar characteristics as the plasma response in the wall-stabilized regime, showing the same perturbed field pattern at the wall and no evidence for island formation provided the plasma is rotating. It is therefore reasonable to assume that the plasma response below the no-wall limit is also linked to the (now ideal MHD stable) $n = 1$ kink mode.

2.4. Dependence of error field tolerance on NBI torque/rotation

Since the error field tolerance is determined by the loss of torque balance, it should improve with increasing torque input to the plasma. The beneficial effect of low power tangential NBI ($P_{\text{NBI}} < 3$ MW) for the error field tolerance has already been observed in previous DIII-D [6] and JET [5] experiments. The DIII-D experiments showed a saturation of the effect at
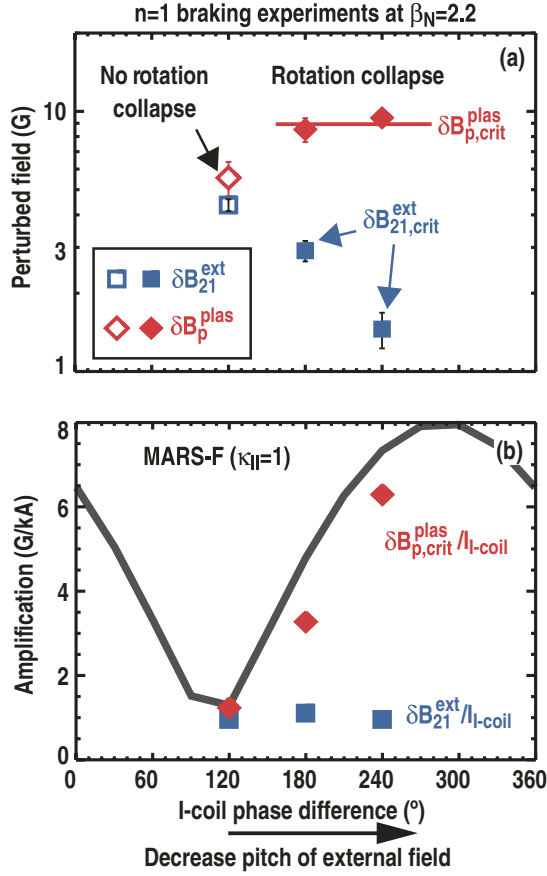
Figure 6. (*a*) Magnetic braking in discharges with constant $\beta_N = 2.2$ ($\approx 1.1\beta_{N,\text{nw}}$) yields the dependence of the $n = 1$ plasma response δB_p^{plas} (diamonds) and the external resonant field at the $q = 2$ surface $\delta B_{21}^{\text{ext}}$ (squares) on the I-coil phase difference $\Delta\phi_I$. The fileds are evaluated at the maximum I-coil current (open symbols) or immediately prior to the rotation collapse (filled symbols). (*b*) The dependence of the amplification $\delta B_p^{\text{plas}}/I_{\text{I-coil}}$ (red diamonds) on $\Delta\phi_I$ is well described by modelling with the MARS-F code (line). Neither the measured nor the modelled plasma response correlate with the resonant component $\delta B_{21}^{\text{ext}}$ (blue squares) of the external field. (Colour online.)

higher NBI power and increased β_N, presumably due to the at that time unknown β_N dependence of the corresponding plasma response. The increase in the tolerable $n = 1$ plasma response with increasing NBI torque even at high values of β_N can already be seen in the β_N scan, figure 4(*b*), described in section 2.2. Assuming a visco-resistive resonant magnetic braking torque $T_R = K_R \delta B_R^2 \Omega^{-1}$ [9], where K_R is a coefficient that depends on plasma parameters and which has the same rotation dependence as the magnetic braking torque T_{MB} in equation (1), the torque balance is lost when the resonant component of magnetic perturbation δB_R exceeds a critical amplitude,

$$\delta B_{R,\text{crit}} = T_{\text{in}} \left(\frac{\tau_{L,0}}{4I K_R} \right)^{1/2}. \quad (2)$$

According to equation (2), the error field tolerance should increase linearly with the torque input T_{in}.

The dependence of the $n = 1$ error field tolerance on the torque input is investigated in similar discharges with T_{NBI} varying from 2 to 6 N m. Increasing T_{NBI} by a factor of three

leads to an increase in the tolerable plasma response $\delta B_{p,\text{crit}}^{\text{plas}}$ by 50%, figure 8(*a*). The onset of a rotating 2/1 NTM prior to the rotation collapse in several discharges led to a modest reduction of the error field tolerance (see open symbols in figure 8(*a*)), which is likely caused by an additional braking torque generated by the interaction of the rotating perturbation with the vessel wall. The measured tolerable plasma response $\delta B_{p,\text{crit}}^{\text{plas}}$ can be easily fitted to a linear dependence on T_{NBI} as suggested by equation (2), albeit with a large torque offset of 8.8 N m. Since discharges with balanced NBI heating, i.e. no net NBI torque, still rotate slowly in the direction of the plasma current there must be an additional anomalous torque T_{an}, which is driving this intrinsic rotation [23]. However, the additional torque of 8.8 N m is too large to be solely explained by T_{an}. Measurements of the angular momentum L_0 before the external non-axisymmetric field is applied, taken at various values of T_{NBI}, yield an estimate of $T_{\text{an}} = 1.4$ N m (figure 8(*b*)). This estimate of T_{an} is in turn used to fit the torque dependence of $\delta B_{p,\text{crit}}^{\text{plas}}$ on $T_{\text{in}} = T_{\text{an}} + T_{\text{NBI}}$, yielding an exponent of 0.45. The T_{in} dependence is, therefore, significantly weaker than the linear dependence expected for a resonant magnetic braking torque, equation (2). The exponent of 0.45 for the torque input dependence of the tolerable plasma response in these DIII-D H-mode experiments resembles observations in NBI heated L-mode discharges in JET, where the scaling of tolerable external field with the rotation Ω_0 at the $q = 2$ surface before the external field is applied yielded an exponent of 0.5 [24]. Assuming that the plasma response in the low power JET discharges ($P_{\text{NBI}} < 2$ MW) is negligible or changes only weakly for the analysed dataset and taking into account that the angular momentum L_0 and therefore Ω_0 in DIII-D is approximately proportional to T_{in} (see figure 8(*b*)), the DIII-D results nicely extend the previous JET findings to H-mode discharges and higher values of β_N. The reduced T_{in} dependence can be explained by a deviation from the Ω^{-1} dependence of T_{MB} due to a significant contribution of non-resonant effects, which will be discussed in section 3.3.

2.5. Comparison of the error field tolerance with the low-density locked mode threshold

The present experiments confirm the key role of the plasma response for the understanding of the $n = 1$ error field tolerance in NBI heated H-modes. Modelling of the perturbed resonant field in the plasma δB_{mn} prior to the rotation collapse using the Ideal Perturbed Equilibrium Code (IPEC) [25] connects the high-β_N error field tolerance determined in the $n = 1$ braking experiments discussed in this paper, with the locked mode threshold measured in Ohmically heated L-modes with low values of β_N. In the ideal MHD model δB_{mn} refers to the field that shielding currents on the $q = m/n$ resonant surface cancel. Previous analysis of low β_N error field correction experiments in DIII-D and NSTX has shown that IPEC calculations of the total perturbed resonant field at the $q = 2$ surface δB_{21} at the onset of locked modes, included in figure 9, restore the well-established linear density scaling [26, 27]. (Note that the values of δB_{21} in figure 9 have been revised since the publication of [26].) The same IPEC modelling of the perturbed $n = 1$ field at the rotation collapse in discharge 127737 at $\beta_N = 1.5$ and an NBI torque

Ideal MHD n=1 RWM (MARS-F)
134234 t = 1750 ms
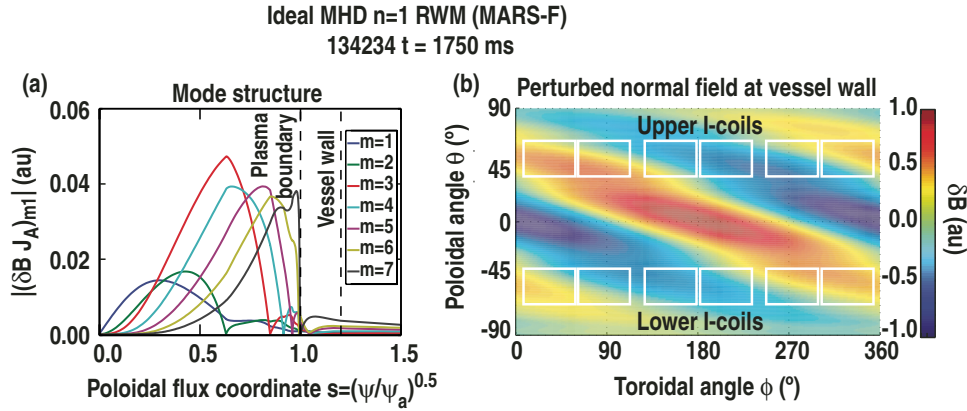
Figure 7. (*a*) The poloidal spectrum (using a straight-field-line coordinate) of the normal component of the perturbed field (multiplied with the surface Jacobian) $(\delta B \cdot J_A)_{mn}$ of an unstable $n = 1$ RWM calculated for 134234 at $t = 1750$ ms with the MARS-F code as a function of a normalized poloidal flux coordinate s shows global kink mode structure. (*b*) The corresponding perturbed normal field δB at the outboard wall best matches an I-coil phase difference $\Delta\phi_I$ between the upper and lower I-coil arrays of approximately 300°.
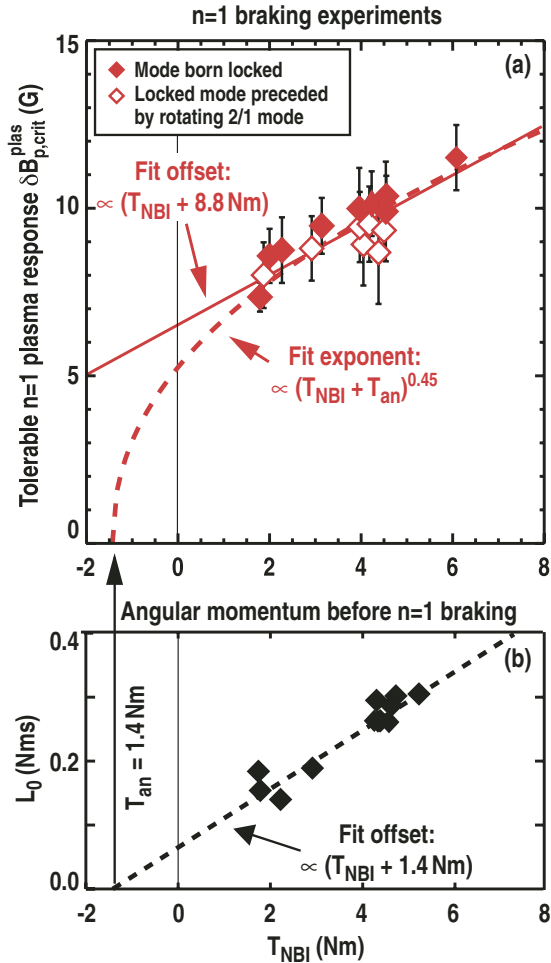
Figure 8. (a) The tolerable $n = 1$ plasma response $\delta B_{p,crit}^{plas}$ evaluated at the rotation collapse in slow magnetic braking experiments increases with increasing NBI torque T_{NBI}. A linear fit (solid) yields a torque offset of 8.8 N m. Fitting the measurement to a power law (dashed) while constraining the torque offset using an estimate for the anomalous torque of $T_{an} = 1.4$ N m, which is (b) obtained from the dependence of the angular momentum L_0 before any external $n = 1$ magnetic field is applied on T_{NBI}, yields an exponent of 0.45.
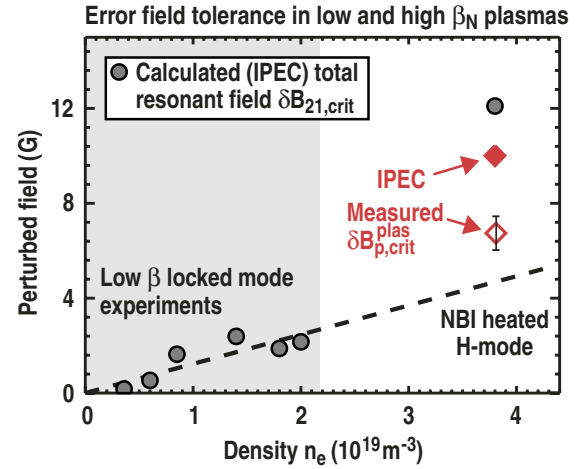
Figure 9. Comparison of IPEC calculations of the total resonant $n = 1$ field at the $q = 2$ surface $\delta B_{21,crit}$ (filled circles) immediately prior to the rotation collapse in an NBI heated H-mode discharge ($\beta_N = 1.5$, $T_{NBI} = 1.8$ N m) with the linear density dependence of the tolerable total field found in Ohmically heated L-mode discharges (shaded) [25]. The calculated plasma response at the sensors (filled diamond) in the NBI heated H-mode exceeds the corresponding measurement (open diamond) by 40%.

$T_{NBI} = 1.8$ N m, shown in figure 3, results in a total resonant field at the $q = 2$ surface of $\delta B_{21} \approx 12$ G, figure 9. With an average electron density of $\langle n_e \rangle = 3.8 \times 10^{19}$ m^{-3} this value for δB_{21} exceeds the extrapolation of the linear density dependence of the error field tolerance in Ohmic plasmas by more than a factor of two, figure 9. This increase in the error field tolerance could be attributed to the beneficial effect of NBI torque. The empirical fit obtained in figure 8 suggests an increase in the error field tolerance in a plasma with $T_{NBI} = 1.8$ N m of approximately 45% over an Ohmically heated plasma with $T_{NBI} = 0$, in qualitative agreement with the result in figure 9.

The IPEC calculation also yields a plasma response at the location of the poloidal field probes at the outboard mid-plane of $\delta B_p^{plas} \approx 10$ G, which exceeds the measured value of 7 G by approximately 40%, figure 9. This comparison represents a first quantitative test of the IPEC model. The agreement can be
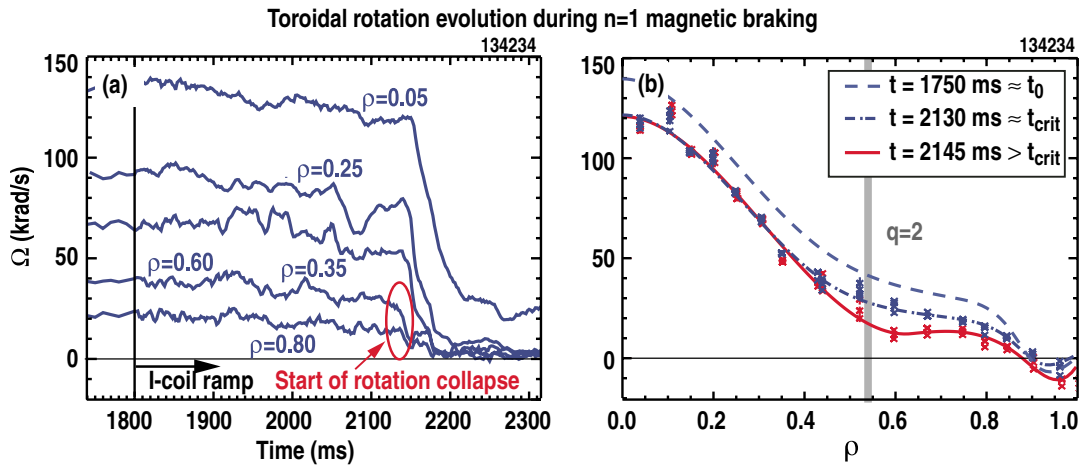
Figure 10. (*a*) Evolution of the toroidal plasma rotation Ω at various minor radii during an $n = 1$ magnetic braking experiment. The red circle highlights the onset of the rotation collapse. (*b*) A comparison between the rotation profiles before the magnetic braking is applied ($t \sim t_0$: dashed) and immediately prior to the rotation collapse ($t > t_{crit}$: dash-dotted) reveals no evidence for a localized braking torque. The rotation collapse then starts in the outer half of the plasma ($t > t_{crit}$: solid). (Colour online.)

significantly improved by removing the outer 4% of poloidal flux from the equilibrium for the IPEC calculations. Further analysis will have to investigate, if such a truncation of the equilibrium is justified. Further uncertainties can arise from the equilibrium reconstruction as well as an observed reduction of the amplification immediately prior to the rotation collapse.

2.6. Consequence of the importance of the plasma response for error field correction

In high β_N discharges experimental observations [15, 28] as well as modelling with the MARS-F code [29] indicate that the response of a stable plasma to externally applied non-axisymmetric fields is well described by a single least stable mode. This means that any externally applied non-axisymmetric field that couples to this mode should be able to oppose the coupling to the intrinsic error field and correct the amplitude of the driven mode to zero, even if the intentionally applied field does not match the structure of the error field. Since the findings reported in sections 2.2–2.5 indicate that the plasma response largely determines the error field tolerance, correction coils even with a poorly matched magnetic field pattern should be effective in suppressing the plasma response and thereby avoid the rotation collapse. This argument only holds as long as the coupling of the external fields to additional modes is negligible and it does not take into account any other adverse effects of non-axisymmetric fields on the plasma performance. A similar conclusion is reached for low beta plasmas based on IPEC analysis, which explains the relatively successful cancellation of intrinsic error fields with the C-coil in DIII-D and the EFC coil in NSTX, despite their lack of control of the poloidal spectrum [26].

3. Magnetic braking

Since the error field limit manifests itself by a loss of torque balance, the error field tolerance is determined by the braking torque that the non-axisymmetric perturbation exerts on the plasma. This work focuses on the rotation braking that leads

to the loss of torque balance rather than the rotation collapse itself.

3.1. Rotation evolution and calculation of the magnetic braking torque

In experiments with slowly increasing $n = 1$ I-coil currents, the toroidal plasma rotation decreases across the entire profile, figure 10(*a*). In addition to a continuous rotation decrease, the rotation measurements taken at a fixed location also oscillate with the externally imposed rotation frequency $f_{ext} = 10$ Hz. This oscillation is caused by a superposition of the externally applied rotating $n = 1$ field with a residual (imperfectly corrected) $n = 1$ intrinsic error field as well as convective transport with the kink-type displacement of the plasma response.

The rotation profile evolution during the slow braking phase does not indicate any evidence of a localized braking torque. A comparison of the rotation profiles before the magnetic braking is applied ($t = 1750$ ms) and immediately prior to the rotation collapse ($t = 2130$ ms) shows the rotation decrease across the entire core of the plasma, figure 10(*b*). The broad rotation damping appears to contradict the resonant braking model, which predicts a highly localized torque at the resonant surfaces. However, diffusive transport, the finite spatial resolution of the rotation measurements and the uncertainty of the measurements limit the detectability of a localized torque. The broad rotation damping is a well-established characteristic of the rotation braking due to amplified externally applied $n = 1$ fields observed in wall-stabilized discharges in DIII-D, JET and NSTX [30]. However, it differs from observations of a localized torque in low β L-modes in JET [24], and is possibly a feature of high β or fast rotating plasmas. In NSTX, the braking due to amplified externally applied $n = 1$ fields has been linked to the non-resonant components of the perturbed field, which according to neoclassical theory result in a broad toroidal braking torque profile [31, 32].
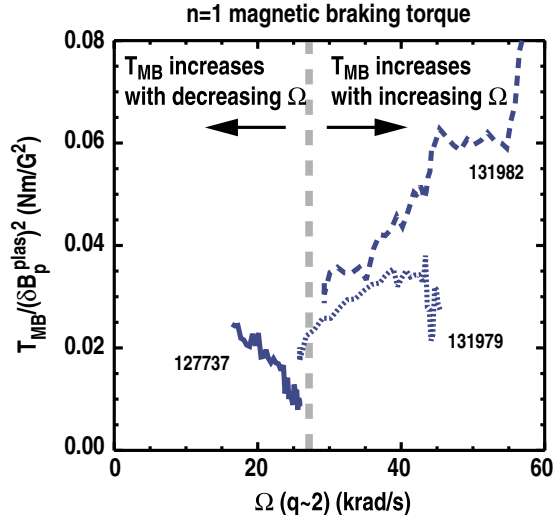
Figure 11. Dependence of the normalized $n = 1$ magnetic braking torque $T_{MB}/(\delta B_p^{plas})^2$, determined from global momentum balance calculations, on the rotation Ω at the $q = 2$ surface. (Colour online.)

Figure 12. Dependence of the rotation Ω_{crit} at the $q = 2$ surface, immediately prior to the loss of torque balance, on the rotation Ω_0 before the $n = 1$ magnetic braking is applied. In these discharges the NBI torque is kept constant throughout the magnetic braking. (Colour online.)

Once the externally applied field exceeds the critical value (at $t = 2135$ ms) the rotation collapse starts in the outer half of the plasma, before it quickly (typically in the order of 10 ms) propagates inwards, figures 10(*a*) and (*b*). This coincides with the region that contains the $n = 1$ resonant surfaces and indicates a rapidly increasing localized braking torque. This observation is at least qualitatively consistent with the model of a resonant torque arising at resonant surfaces when the decreasing rotation leads to a loss of the shielding currents thought to be responsible for the rotation collapse.

3.2. Frequency dependence of the torque

While it is difficult to determine the torque density profile, an estimate of the total magnetic braking torque T_{MB} is obtained from the measured global rotation evolution,

$$T_{MB} = T_{in} - \frac{L}{\tau_{L,0}} - \frac{dL}{dt}. \tag{3}$$

The profiles for the transport calculations, which have been carried out with the TRANSP code [14], are averaged over the externally imposed oscillation period of 100 ms in order to suppress the non-axisymmetric effects on the measurements discussed above, which are not part of the transport calculation. The only source of rotation contributing to T_{in} in the transport calculation is the NBI torque. Since most magnetic torque models rely on a $\delta j \times \delta B$ torque, where δj is induced through δB, it is tenable to assume that the magnetic torque has a $(\delta B)^2$ dependence. Here, δB is the perturbed field in the plasma. Since sections 2.2 and 2.3 have shown that in the analysed parameter range the braking torque is determined by the measured plasma response δB_p^{plas}, the measurement taken outside the plasma should be proportional to the perturbed field inside the plasma. Normalizing T_{MB} with $(\delta B_p^{plas})^2$ therefore reveals the Ω dependence, which is shown for Ω at the $q = 2$ surface for several discharges in figure 11. While the discharge with the lowest rotation shows a torque that increases with decreasing Ω the high rotation discharges reveal
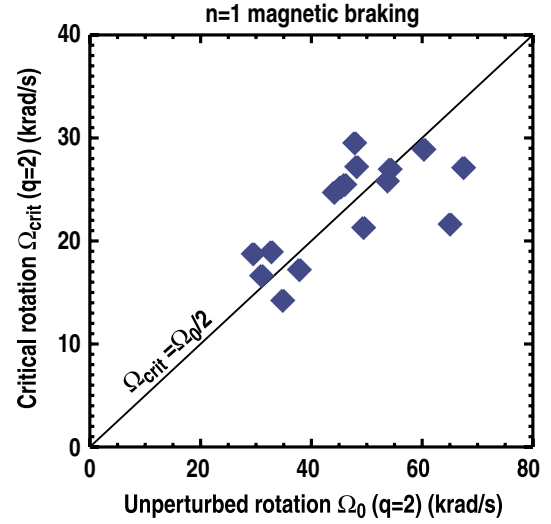
a torque that increases with increasing Ω. The lowest torque is encountered when the rotation evaluated at the $q = 2$ surface is approximately $25 \, \text{krad s}^{-1}$.

3.3. Simultaneous resonant and non-resonant braking

The imperfect shielding of resonant components of the perturbed field leads to a resonant braking torque, which typically depends on Ω^{-1} [9]. In addition to this resonant braking, neoclassical theory predicts that the non-resonant components of the perturbed field also lead to a braking torque, which typically increases proportionally with Ω and is referred to as neoclassical toroidal viscosity [31]. The frequency dependence of the braking torque, shown in section 3.2 and figure 11, is therefore another indication (in addition to the broad rotation damping profile described in section 3.1) that non-resonant effects are important to describe the error field tolerance, in particular, in fast rotating plasmas. Since the actual Ω dependences for resonant and non-resonant braking torques depend on the parameter regime, this work refers to a torque $T_R = K_R \delta B_R^2 \Omega^{-1}$ as 'resonant-like' and to $T_{NR} = K_{NR} \delta B_{NR}^2 \Omega$ as 'non-resonant-like' torque, with δB_R and δB_{NR} being the corresponding relevant components of the non-axisymmetric field. This functional form of T_{NR} does in particular neglect the effect of a neoclassical offset rotation [33, 34], which becomes important at low rotation and high ion temperatures. Adding a non-resonant-like torque to the typical resonant-like magnetic braking torque in the angular momentum evolution, equation (1),

$$I\frac{d\Omega}{dt} = T_{in} - \frac{I\Omega}{\tau_{L,0}} - K_{NR}\delta B_{NR}^2\Omega - K_R\delta B_R^2\Omega^{-1}, \tag{4}$$

results in a decrease in the rotation at the collapse from the characteristic $\Omega_{crit} = \Omega_0/2$ of the resonant braking model (assuming that all other torques stay constant and that the viscous momentum transport is described by a momentum

confinement time) to

$$\Omega_{\rm crit} = \frac{1}{2}\frac{\tau_{\rm L^*}}{\tau_{\rm L,0}}\Omega_0. \tag{5}$$

The effective momentum confinement time $\tau_{\rm L^*} = (\tau_{\rm L,0}^{-1} + I^{-1}K_{\rm NR}\delta B_{\rm NR}^2)^{-1}$ in equation (5) accounts for the confinement reduction caused by non-resonant-like magnetic braking. Note that any non-resonant braking that is present before the I-coil ramp is already accounted for in $\tau_{\rm L,0}$. In experiments where $T_{\rm NBI}$ is kept constant, the critical rotation $\Omega_{\rm crit}$ indeed indicates a deviation from the simple scaling with $\Omega_{\rm crit}$ at the highest initial rotation values Ω_0 falling below $\Omega_0/2$, as seen in figure 12. Moreover, $\Omega_{\rm crit}$ never exceeds 30 krad s^{-1}, which is close to the minimum of the torque shown in figure 11.

While a non-resonant torque alone cannot cause a bifurcation in the torque balance, it reduces the tolerable resonant field:

$$\delta B_{\rm R,crit} = T_{\rm in}\left[\tau_{\rm L^*}/(4IK_{\rm R})\right]^{1/2}. \tag{6}$$

In the limit of large $\delta B_{\rm NR} \gg [I/(K_{\rm NR}\tau_{\rm L,0})]^{1/2}$ the tolerable resonant field becomes

$$\delta B_{\rm R,crit} = T_{\rm in}\delta B_{\rm NR}^{-1}(4K_{\rm R}K_{\rm NR})^{-1/2}. \tag{7}$$

The plasma response is expected to have resonant and non-resonant components, $\delta B_{\rm R}$ and $\delta B_{\rm NR}$, which are both proportional to $\delta B_{\rm p}^{\rm plas}$. Substituting $\delta B_{\rm NR}$ in equation (7) with $\delta B_{\rm p}^{\rm plas}$ then yields that the linear dependence of $\delta B_{\rm R,crit}$ on $T_{\rm in}$ motivated by equation (2) is reduced to $\delta B_{\rm p,crit}^{\rm plas} \propto T_{\rm in}^{0.5}$. The observed dependence of $\delta B_{\rm p,crit}^{\rm plas} \propto T_{\rm in}^{0.45}$ in section 2.4 and figure 9 is, therefore, consistent with a strong contribution of non-resonant braking. Note that, since equation (7) is only valid for large $\delta B_{\rm NR}$, which is assumed to be proportional to $\delta B_{\rm p}^{\rm plas}$, the simple relation between $\delta B_{\rm p,crit}^{\rm plas}$ and $T_{\rm in}$ is also only valid for large $\delta B_{\rm p,crit}^{\rm plas}$, too.

4. Conclusion and summary

The limit to tolerable externally applied $n = 1$ 'error' fields in tokamak plasmas is caused by resonant magnetic braking leading to a bifurcation in the torque balance, which is followed by an error field-driven locked mode. The error field tolerance can be improved by increasing the applied torque, e.g. with tangential NBI. Non-resonant effects are observed to reduce the beneficial effect of additional torque input. The error field tolerance decreases with increasing $\beta_{\rm N}$. The importance of this $\beta_{\rm N}$ dependence in particular for low torque scenarios was not previously appreciated, and was not included in the empirical scaling of the error field tolerance reported in the ITER Physics Basis [1, 2], which focused on the lowest density phase of a discharge prior to H-mode access. The $\beta_{\rm N}$ dependence is explained by the dominant role of the plasma response to the externally applied field in the braking. Experiments applying external fields with various poloidal spectra and the corresponding modelling using the MARS-F code, both show that the plasma response is caused by a resonant amplification of the stable $n = 1$ kink mode. The plasma is most sensitive to

an external field that matches the structure of the kink mode, which is not necessarily an external field with a large pitch resonant component. The first quantitative benchmarking of the ideal MHD code IPEC shows that the measured plasma response is in reasonable agreement with predictions. The rate of increase in the amplification with $\beta_{\rm N}$ becomes larger above the ideal MHD no-wall stability limit, where kinetic effects stabilize the RWM. This has three important consequences for the (re-)evaluation of the error field tolerance in ITER. (1) Neglecting the $\beta_{\rm N}$ dependence in empirical scaling can lead to overly optimistic predictions for low torque, high $\beta_{\rm N}$ scenarios and, in particular, for advanced tokamak scenarios, which rely on operation in the wall-stabilized regime. (2) The error field tolerance has to be specified for the component that couples best to the kink mode, which at least at the outboard mid-plane has a lower pitch angle than the $n = 1$ field that is resonant with rational surfaces inside the plasma and currently used for empirical scaling laws. (3) Correction coils, even with a poorly matched magnetic field pattern, may be effective in suppressing the plasma response and avoiding a rotation collapse, as was suggested by numerical plasma response calculations for ITER [35]. The measurable increase in the plasma response with $\beta_{\rm N}$ can then be exploited for 'dynamic' correction of the field error using slow magnetic feedback.

References

[1] 1999 ITER Physics Basis *Nucl. Fusion* **39** 2137
[2] Hender T.C *et al* 2007 *Nucl. Fusion* **47** S128
[3] La Haye R.J. *et al* 1992 *Phys. Fluids* B **4** 2098
[4] Hender T.C. *et al* 1992 *Nucl. Fusion* **32** 2091
[5] Buttery R.J. *et al* 1999 *Nucl. Fusion* **39** 1827
[6] La Haye R.J., Hyatt A.W. and Scoville J.T. 1992 *Nucl. Fusion* **32** 2119
[7] Garofalo A.M. *et al* 2007 *Nucl. Fusion* **47** 1121
[8] Garofalo A.M. *et al* 2007 *Bull. Am. Phys. Soc.* **52** 101
[9] Fitzpatrick R. 1993 *Nucl. Fusion* **33** 1049
[10] Reimerdes H. *et al* 2007 *Plasma Phys. Control. Fusion* **49** B349
[11] Buttery R.J. *et al* 2008 *Phys. Plasmas* **15** 056115
[12] Buttery R.J. *et al* 2008 *Proc. 22nd Int. Conf. on Fusion Energy 2008 (Geneva, Switzerland, 2008)* (Vienna: IAEA) CD-ROM file IT/P6-8 and http://www-naweb.iaea.org/napc/physics/FEC/FEC2008/html/index.htm
[13] Glasser A.H. and Chance M.S. 1997 *Bull. Am. Phys. Soc.* **42** 1848
[14] Hawryluk R. 1980 *Physics of Plasmas Close to Thermonuclear Conditions* vol 1 ed B. Coppi *et al* (Brussels: CEC) pp 19–46
[15] Garofalo A.M. *et al* 2002 *Phys. Plasmas* **9** 1997
[16] Hender T.C. *et al* 2004 *Proc. 20th Int. Conf. on Fusion Energy 2004 (Vilamoura, Portugal, 2004)* (Vienna: IAEA) CD-ROM file EX/P2-22 and http://www-naweb.iaea.org/napc/physics/fec/fec2004/datasets/index.html
[17] Sabbagh S.A. *et al* 2006 *Nucl. Fusion* **46** 635
[18] Boozer A.H. 2001 *Phys. Rev. Lett.* **86** 5059
[19] Hu B. and Betti R. 2004 *Phys. Rev. Lett.* **93** 105002

[20] Liu Y.Q., Bondeson A., Fransson C.M., Lennartson B. and Breitholtz C. 2000 *Phys. Plasmas* **7** 3681
[21] Bondeson A. and Chu M.S. 1996 *Phys. Plasmas* **3** 3013
[22] Bondeson A. and Ward D.J. 1994 *Phys. Rev. Lett.* **72** 2709
[23] deGrassie J.S., Rice J.E., Burrell K.H., Groebner R.J. and Solomon W.M. 2007 *Phys. Plasmas* **14** 056115
[24] Lazzaro E. *et al* 2002 *Phys. Plasmas* **9** 3906
[25] Park J.-K., Boozer A.H. and Glasser A.H. 2007 *Phys. Plasmas* **14** 052110
[26] Park J.-K., Schaffer M.J., Menard J.E. and Boozer A.H. 2007 *Phys. Rev. Lett.* **99** 195003
[27] Park J.-K. *et al* 2009 *Phys. Plasmas* **16** 056115
[28] Reimerdes H. *et al* 2004 *Phys. Rev. Lett.* **93** 135002
[29] Liu Y.Q. *et al* 2006 *Phys. Plasmas* **13** 056120
[30] Reimerdes H. *et al* 2006 *Phys. Plasmas* **13** 056107
[31] Shaing K.C. 2003 *Phys. Plasmas* **10** 1443
[32] Zhu W. *et al* 2006 *Phys. Rev. Lett.* **96** 225002
[33] Cole A.J., Hegna C.C. and Callen J.D. 2007 *Phys. Rev. Lett.* **99** 065001
[34] Garofalo A.M. *et al* 2008 *Phys. Rev. Lett.* **101** 195005
[35] Park J.-K., Boozer A.H., Menard J.E. and Schaffer M.J. 2008 *Nucl. Fusion* **48** 045006